Vibrational Energy Dynamics of Glycine, *N*-Methylacetamide, and Benzoate Anion in Aqueous (D_2O) Solution

Ying Fang, Shinsuke Shigeto,† Nak-Hyun Seong, and Dana D. Dlott*

School of Chemical Sciences, University of Illinois at Urbana−Champaign, Urbana, Illinois 61801

Received: July 14, 2008; Revised Manuscript Received: September 17, 2008

Ultrafast infrared-Raman spectroscopy is used to study vibrational energy dynamics of three molecules in aqueous solution (D_2O) that serve as models for the building blocks of peptides. These are glycine-d_3 zwitterion (GLY), *N*-methylacetamide-*d* (NMA), and benzoate anion (BZ). GLY is the simplest amino acid, NMA a model compound with a peptide bond, and BZ a model for aromatic side chains. An ultrashort IR pulse pumps a parent CH-stretch on each solute. Anti-Stokes Raman monitors energy flow through the solutes' strongly Raman-active transitions. Stokes Raman of D_2O stretching functions as a molecular thermometer to monitor energy dissipation from solute to solvent. A three-stage model is used to summarize the vibrational energy redistribution process and to provide a framework for discussing energy dynamics of different molecules. The initial CH-stretch excitation is found to be delocalized over some or all of the solute molecule in NMA and BZ but not in GLY. The overall time constants for energy dissipation are 7.2 ps for GLY, 4.9 ps for NMA, and 8.0 ps for BZ. CH-stretch energy in GLY is redistributed in a nearly statistical manner among observed GLY vibrations. In NMA the energy is distributed among about one-half of the observed vibrations, and in BZ much of the observed energy is channeled along a CH-stretch to the ring stretch pathway. The strongly Raman-active vibrations accurately represent the flow of vibrational energy through NMA but not through GLY or BZ.

1. Introduction

In this study we discuss a "bottom-up" approach to the problem of vibrational energy in proteins via a detailed study of the simpler building blocks. The ultrafast infrared-Raman (IR-Raman) technique[1,2] was used to investigate vibrational energy flow of three biologically relevant molecules in aqueous (D_2O) solution: glycine (GLY), the simplest amino acid in the form glycine-d_3 zwitterion; *N*-methylacetamide-*d* (NMA), a model compound with a peptide bond; benzoate anion (BZ), a model for peptide aromatic side chains. In these IR-Raman measurements, a CH-stretch transition was pumped by a short-duration IR pulse, and a time series of anti-Stokes Raman spectra were acquired to measure the time-dependent populations of the parent excitation and the daughter excitations created by parent vibrational relaxation (VR). The vibrational cooling (VC) process is monitored by observing the Raman spectrum of the aqueous medium,[3,4] which functions as a molecular thermometer.[5−7] In the VC process studied here, a solution initially at temperature T_i is pumped by an IR pulse that excites solute molecules but not solvent molecules. As the solute molecules lose their excess vibrational energy to the surroundings, the solution comes to equilibrium at a temperature T_f a few K above T_i.

Most prior studies of vibrational energy in proteins have utilized a "top-down" approach to energy dissipation mechanisms which could be relevant to biological function such as enzyme catalysis. Well-known examples include myoglobin, hemoglobin, or cytochrome c where heme has been electronically excited.[7−14] The excitation is converted to heme vibrational energy in ∼5 ps, and the heme cools by 20−40 ps energy transfer through the protein into the aqueous medium.[7−11,15] Heme cooling has been monitored using transient gratings,[16] resonance anti-Stokes Raman measurements of the heme,[9−12,17,18] ultraviolet resonance Raman measurements of the globin,[19−21] and IR absorption of the aqueous medium as a molecular thermometer.[7] Experimental[20] and theoretical[15,22−24] studies have suggested that energy can be funneled from a hot porphyrin, through its side chains, into specific parts of the protein.

"Bottom-up" approaches to protein vibrational energy have used IR pump−probe techniques to study the vibrational relaxation of small ligands such as CO bound to the active sites of heme proteins,[25−28] or the peptide backbone[29] itself via the amide I mode,[29−32] which is predominantly a CO stretching excitation.

Recently our group used IR-Raman to study glycine[33] in H_2O with a CH-stretch parent excitation at 2980 cm^{-1}. The anti-Stokes results were analyzed using a three-stage model for VC discussed in detail below. The three stages were a 0.8 ps decay of the parent, which populated both midrange and lower-energy vibrations, a 1.0 ps relaxation of the midrange vibrations, and a 1.2 ps relaxation of the lower-energy vibrations. The net cooling process observed via water molecular thermometer was described by a 1.8 ps time constant.

The interpretation of the glycine work and the present work raises several important issues.

(1) What is the nature of the initial state? The IR pulse excites a state which is nominally a CH-stretch excitation but is really a "bright" state, i.e. a combination of eigenstates of the harmonic Hamiltonian with a large transition dipole that has some CH-stretch character. The bright state, or parent excitation, is anharmonically coupled to tiers of lower-energy excitations that become progressively more distant in state space.[34−37] Thus vibrational transitions that we tend to view as local modes are frequently delocalized over many atoms. This issue is germane

* Corresponding author. E-mail: dlott@scs.uiuc.edu.
† Present address: Department of Applied Chemistry, National Chiao Tung University, 1001, Ta-Hsueh Road, Hisnchu 30010, Taiwan.

10.1021/jp8062228 CCC: $40.75
Published on Web 12/09/2008

to the emerging use of direct probes of protein vibrations[38] by isotope labeling, for instance using 2D IR techniques[31,39,40] to probe CD-labeled amino acids or peptides.[41,42] The IR-Raman method provides a method to disentangle the nature of the initial state and the time-dependent energy transfer processes that result from successive tiers of anharmonic couplings.

2. How representative are the probed excitations? The IR-Raman method is the best available technique for watching vibrational energy flow in molecules, but with a very few exceptions (water,[43] chloroform,[44] nitromethane[45]) the Raman probe sees only a portion of all molecular vibrations. The molecules studied here, GLY, NMA, and BZ, have 10, 12, and 14 atoms, giving 24, 30, and 36 normal modes of vibration, but in the most favorable case (NMA) we have the sensitivity to probe only 9 of them. The molecules one studies might fall into two classes. The observed vibrational energy might be representative or nonrepresentative of the total molecular energy. We will show here that we can accurately determine this for the molecules studied. A representative molecule would be a more useful and accurate probe of protein vibrational energy.

3. What language can be used to describe energy dissipation? The VR process can be described by a master equation that includes a matrix of state-to-state rate constants.[45−47] For glycine, for instance, this would be a 24 × 24 matrix. Such a description has been obtained for $CHCl_3$ and CH_3-CN, but it becomes overly complex for larger molecules and does not promote a cohesive intuitive picture. In addition it does not facilitate discussions comparing two different molecules, solvent effects, isotopic substitution, and so forth. For many years the "vibrational cascade" was used to describe the cooling of vibronically excited condensed-phase molecules.[48] Vibrational cascade is a good description for VR of high-lying vibrational states of diatomic molecules in condensed phases. A molecule such as XeF in solid Ar might be prepared in $v = 20$ and then cascade down the ladder of lower v-states until cooled.[49] But with larger polyatomic molecules, IR-Raman and hot fluorescence measurements did not observe this type of successive-stepladder descent,[48] because energy from the parent excitation tended to randomize rather than descend a ladder. Recently our group has introduced a three-stage model[33,45] for VC of condensed-phase molecules where the initial excitation has enough energy that the primary decay pathway is intramolecular vibrational redistribution (IVR).[33,45] Studies of gas-phase molecules indicate this occurs when the state density is in the 10^2-10^3 states/cm^{-1} range, which ought to be the case for CH-stretching excitations of molecules with 4−5 or more heavy (not H or D) atoms.[50] The three-stage model, discussed in detail in the next section, has been successfully used to describe VR of nitromethane[45] and of glycine[33] in aqueous solution. In what follows we will use this model to describe the VR of GLY, NMA, and BZ in deuterated water and show that it is a consistent and useful picture of vibrational energy flow in such systems.

2. Three-Stage Model for Vibrational Energy Flow

This model should prove useful for molecules the size of biological building blocks such as amino acids, nucleic acids, simple sugars, and so on. For the model to apply, the molecules must be large enough that the parent excitation at ~3000 cm^{-1} decays via IVR. The model will not be useful for smaller molecules, since the initial VR step would depend on fine details of the intermolecular potential and would be difficult to predict in advance.[48] The model would also not be useful for much larger molecules, say a peptide with many amino acids. The model might well be a good description of VR occurring locally,

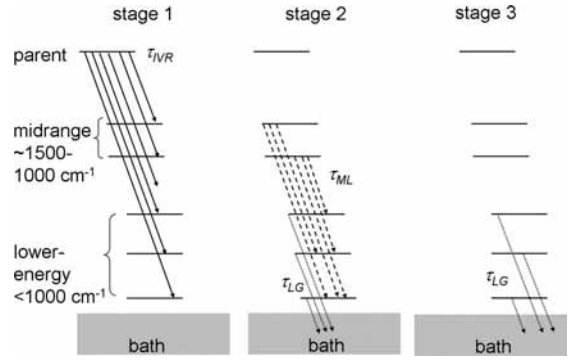

Figure 1. Schematic of the three-stage model for vibrational cooling (VC). Stage 1: A parent vibration P such as a CH-stretch is excited. P is above the threshold for intramolecular vibrational redistribution (IVR). IVR with lifetime τ_{IVR} populates many or perhaps all the lower vibrations. Stage 2: the midrange tier M undergoes vibrational relaxation (VR) with lifetime τ_{ML} by exciting lower-energy vibrations L plus excitations of the bath, while the lower-energy tier undergoes VR with time constant τ_{LG} (G denotes ground vibrational state) by exciting only bath excitations. Stage 3: Lower-energy vibrations created in stage 2 undergo relaxation with time constant τ_{LG}.

but it would not describe the global energy transfer process since the model posits that the initial IVR process redistributes the parent excitation among many or most of the molecule's vibrations, whereas in a large molecule the initially excited CH-stretch excitation would not couple very well to vibrations on distant parts of the molecule.

In the model, which is depicted in Figure 1, we divide the vibrations into three tiers: the parent P, the midrange levels M, and the lower energy levels L. The bath consists of the lower-energy continuum of collective excitations of the solute and aqueous medium. The assignment of intermediate and lower-energy levels is based on the work of Nitzan and Jortner.[51] The M vibrations are characterized as being mostly harmonic excitations residing in an energy region with higher state density, whereas the L vibrations are more anharmonic lower-energy bending or deformation modes residing in an energy region of lower state density. Typically the midrange vibrations of organic molecules would be in the 1700−1200 cm^{-1} range and the lower energy-vibrations below 1200 cm^{-1}, but this is not always a sharp distinction,[48] depending for instance on how rigid is the molecular framework. For simplicity, we assume that VR process subsequent to parent decay can be described by two rate constants, one for the M tier and one for the L tier. In other words our model assumes that variations in the lifetimes of the individual states in the M and L tiers are small. In the event that one of the states in these tiers has a radically different lifetime from the others, the model can be patched up by including this state explicitly, but if there are too many of these outlying states, it would probably be more worthwhile to use a model that considers each state explicitly.

The first stage is relaxation of the excitation P produced by laser pumping. The pumping rate is $\alpha J(t)$, where α is the absorption coefficient and $J(t)$ the time-dependent fluence (photons m^{-2}) of the IR pump pulse. Subsequent to thermalization the net temperature jump $\Delta T = \int dt J(t)\alpha/C$, where C is the solution heat capacity.[52] In practice the temperature jump is spatially inhomogeneous in both longitudinal and transverse directions, so we experimentally determine an effective spatially averaged ΔT using data[53] from anti-Stokes transients at longer times after a new equilibrium has been reached. Other vibrations which contribute to the character of the bright state P will also be pumped directly by the laser, and these states are described[54−57] as "coherently coupled" to P.

We use the term "coherently coupled" states to describe vibrational excitations that are coupled to the parent bright state by an interaction $\langle V \rangle$ which is about equal to or greater than $(T_2)^{-1}$ where T_2 is the time constant for dephasing.[55,57] In order to understand the effects of this coupling, consider the familiar case of a 2:1 Fermi resonance of CH-stretch and bend. The laser initially excites a state with mainly stretch character, but this state evolves into a mixed stretch−bend state. This is a kind of IVR process, but we prefer not to use the term "IVR" to avoid confusion with the T_1 relaxation which is also intramolecular. When the time resolution is high, this time evolution usually takes the form of damped quantum beats, which are well-known in both vibronic spectroscopy[58] and ultrafast IR spectroscopy.[59] As discussed previously,[60] in our anti-Stokes experiments, IR excitation is semiimpulsive, i.e. the pulse duration is long compared to the vibrational period, comparable to T_2 and shorter than T_1, so we are probing vibrational populations in the parent and coupled states averaged over a time period $\sim T_2$ and not resolving quantum beats. Ordinarily, in quantum beat measurements, the probe pulse is sensitive to either the parent or the coupled states, so as the population oscillates among them, the signal intensity also oscillates. In anti-Stokes Raman the probe situation is a bit different, because in anti-Stokes Raman where the probe bandwidth is greater than the anharmonic coupling, an overtone looks like a fundamental excitation with twice the amplitude and a combination band appears as excitation of both states.[44] For instance with the 2:1 Fermi resonance, we would see a CH-stretch at $\sim$3000 cm^{-1} via the $\upsilon = 1 \rightarrow 0$ transition and a CH-bend at $\sim$1500 cm^{-1} via the $\upsilon = 2 \rightarrow 1$ transition. Thus in our anti-Stokes Raman experiments, "coherent coupling" is observed as instantaneous excitation of lower-energy vibrations that can combine with other vibrations to produce states near the parent energy. The parameters α' and α'', which most often are zero, characterize the rates at which M or L vibrations respectively become excited by coherent coupling with IR pumping of P.

After the initial excitation is prepared, the population in P decays via IVR with time constant τ_{IVR}. This IVR process results in little or no energy dissipated to the bath. Parent IVR excites many midrange M and lower-energy L vibrations. In fact we will provide evidence to show that IVR excites every observed M and L vibration. However the M and L vibrations become excited to different extents which depend on the detailed intermolecular couplings. Let the subscript i denote vibrations in the M tier and the subscript j vibrations in the L tier. Then ϕ_{PMi} is the quantum efficiency for IVR from P to mode i of the M tier, and ϕ_{PLj} is the quantum efficiency from P to mode j of the L tier.

In the second stage, the excited M and L vibrations decay but with different mechanisms. The M vibrations decay with time constant τ_{ML} by exciting L vibrations plus the bath. The lower-energy vibrations decay with time constant τ_{LG} (G denotes vibrational ground state) by exciting the bath only. The quantum efficiency for transfer from mode i of the midrange tier to mode j of the lower-energy tier is ϕ_{MiLj}. However, we do not experimentally determine which specific M vibration excites a specific L vibration, so we can measure only the net quantum efficiency of transfer from all M modes to mode L_i, $\phi_{MLj}\sum_i M_i(t) = \sum_i \phi_{MiLj} M_i(t)$.

In the third stage there is no excitation left in either P or M. The remaining L excitations decay into the bath with time constant τ_{LG}. In the model we assume all vibrations in the M tier have the same lifetime τ_{ML} and all vibrations in the L tier the same lifetime τ_{LG}. We are saying lifetime variations within the M and L tiers are small, and if they are not, the model fails and additional parameters must be introduced. Thus the VR process is described by three global rate constants $k_{\mathrm{IVR}} = (\tau_{\mathrm{IVR}})^{-1}$, $k_{ML} = (\tau_{ML})^{-1}$ and $k_{LG} = (\tau_{LG})^{-1}$.

The three-stage model is summarized by the following set of equations,

$$\frac{dP(t)}{dt} = -k_{\mathrm{IVR}}[P(t) - P^{\mathrm{eq}}] + \alpha J(t)$$

$$\frac{dM_i(t)}{dt} = k_{\mathrm{IVR}}\varphi_{PMi}[P(t) - P^{\mathrm{eq}}] - k_{ML}[M_i(t) - M_i^{\mathrm{eq}}] + \alpha'_i J(t)$$

$$\frac{dL_j(t)}{dt} = k_{\mathrm{IVR}}\varphi_{PLj}[P(t) - P^{\mathrm{eq}}] + k_{ML}\varphi_{MLj}\sum_i [M_i(t) - M_i^{\mathrm{eq}}] - k_{LG}[L_j(t) - L_j^{\mathrm{eq}}] + \alpha''_j J(t) \quad (1)$$

In eqs 1, the superscript eq denotes thermal equilibrium population at the final temperature T_{f}. Although we determine the quantum efficiencies ϕ_{PMi}, ϕ_{PLj}, and ϕ_{MLj} directly, since we do not detect many of the molecular vibrations we have found it convenient to normalize the observed vibrational energy using the conditions $\sum\phi_{PMi} + \sum\phi_{PLj} = 1$, and $\sum\phi_{MLj} = 1$. By way of example, if we observe two M vibrations and one L vibration having the same quantum efficiency for transfer, then $\phi = 0.33$ for each vibration, even though a great deal of energy might also be present in unobserved vibrations.

The three stages participate differently in the VC process. The first stage is purely an IVR process, so little or no energy is dissipated to the bath. The second $M \rightarrow L$ stage is responsible for the smaller part of VC because the energies being dissipated are the difference between the M and L energies. For instance an $M \rightarrow L$ relaxation might involve a 1500 cm^{-1} M vibration which decays by exciting a 1000 cm^{-1} L vibration plus 500 cm^{-1} of bath excitation. The greater part of VC is the $L \rightarrow G$ relaxation process, since all the energy of the L excitation is converted into bath excitations.

An anti-Stokes transient is generated using both Stokes and anti-Stokes data. First we subtract the ambient temperature signal (obtained at a negative delay time when probe precedes pump) and then we divide by the Stokes intensity. An anti-Stokes transient represents the time-dependent change in vibrational occupation number induced by a pump pulse. According to eq 1, the time dependence of an anti-Stokes transient can be thought of as having three parts, a rise, a decay, and a longer-time plateau. The rise provides information about how the vibration was pumped. The rising edge is therefore the key to understanding the flow of vibrational energy. The decay yields the vibrational lifetime T_1. This lifetime is proportional to the amplitude of the Fourier component at the vibrational frequency of the fluctuating forces exerted by the surroundings.[61,62] The plateau reflects the overall increase in excited vibrational population due to the bulk temperature jump ΔT.

Equations 1 are complicated and contain many parameters. In particular the rising edges of the transients are predicted to be quite complicated. For instance the rising edges of the L vibrations could potentially be triexponential, with a component from direct laser pumping, from IVR and from M to L energy transfer. Our signal-to-noise ratio is not sufficient to resolve such a complicated function. However, in practice it is not difficult to evaluate the anti-Stokes transients and determine the parameters in eqs 1 using the following systematic method, which is performed in an iterative, self-consistent fashion.

(1) We first determine the laser apparatus time response function using nonlinear light scattering from water or D_2O.

The laser response $f(t)$ is a good fit to a Gaussian function with fwhm of 1.4 ps. (2) The values P^{eq}, M_i^{eq}, and L_j^{eq} are simply the longer-time plateau values of each anti-Stokes transient.[63] (3) We fit the parent decay, with the nonlinear light scattering contribution removed as described previously[60,64,65] with the convolution of the laser response and an exponential function to determine τ_{IVR}. P_{eq} is close to zero and can be ignored. (4) We find decay lifetimes τ_{ML} and τ_{LG} for the M and L tiers that do a good job of fitting all the transients within each tier. (5) We examine each L and M transient's rising edge. Any rise that demonstrates a component faster than τ_{IVR} is identified as being coherently coupled with the parent excitation and therefore having a nonzero value of α' or α''. (6) We fit the M transients using the parameters determined above while varying the value of ϕ_{PM} for each transient. If a transient has a nonzero α' that is also included in the fit. VII. We fit the L transients by varying the values of both ϕ_{PL} and ϕ_{ML} for each transient. All the values of α'' were found to be zero, so this parameter was not used. Since we need two quantum efficiencies to fit each L transient, the values of ϕ_{PL} and ϕ_{ML} have the greatest experimental uncertainties.

To summarize, after the apparatus response and ΔT are determined, the τ_{IVR}, τ_{ML}, and τ_{LG} lifetimes are extracted from the decaying parts of the P, M, and L transients, respectively. The risetimes of each M_i transient are fit with one adjustable parameter, ϕ_{PMi}. The risetimes of each L_j transient are fit with two adjustable parameters, ϕ_{PLj} and ϕ_{MLj}. Any transient that demonstrates a rise too fast to be fit by these methods is deemed to be coherently coupled with the parent, and an additional coupling parameter α' or α'' is then included.

3. Experimental Section

A. Materials. D_2O (99.9%-D) was purchased from Cambridge Isotope Laboratories and used as received. Sodium benzoate (99%) was purchased from Fluka and used as received. *N*-methylacetamide (99%) was purchased from Aldrich and recrystallized once. Glycine (99%) was purchased from Sigma-Aldrich, recrystallized, and partially deuterated by isotope exchange in D_2O, yielding d_3-glycine. These three solids, GLY, NMA, and BZ, were dissolved in D_2O at a concentration of 2.0 M. In solution, GLY is present as the d_3-glycine zwitterion, $ND_3^+-CH_2-CO_2^-$, NMA is present in the NMA-*d* form, $CH_3-CO-ND-CH_3$ (a small amount of HOD impurity was produced due to exchange between NMA and D_2O), and BZ is present as the benzoate anion, $C_6H_5CO_2^-$.

B. Laser System. The 1 kHz laser apparatus for the IR-Raman experiments has been described previously.[66] A schematic diagram is shown in Figure 2. A tunable mid-IR pulse (~1.0 ps duration, 25 cm^{-1} bandwidth, 200 μm diameter, 10 μJ energy) pumped a recirculating liquid jet ~100 μm thick with a D_2O solution of GLY, NMA, or BZ. The IR pulse was tuned to CH-stretch absorptions at 2970 cm^{-1} for GLY, 2950 cm^{-1} for NMA, and 3050 cm^{-1} for BZ. The temperature jump ΔT was ≤10 K in each case. A time-delayed 532 nm probe pulse (~1.0 ps duration, 25 cm^{-1} bandwidth, 80 μm diameter, 20 μJ energy) was used to generate Raman scattering, which was detected with a multichannel spectrograph and CCD detector over the −3800 to +3800 cm^{-1} range. At each delay time, a 3 min integration time was used.

C. Laser Apparatus Time Response. The laser apparatus time response was measured using incoherent nonlinear light scattering (NLS) from pure D_2O at the frequency IR + visible, as described previously.[3,43,67] The time dependence of the NLS signal was fit by a Gaussian function with fwhm 1.4 ps.[66]

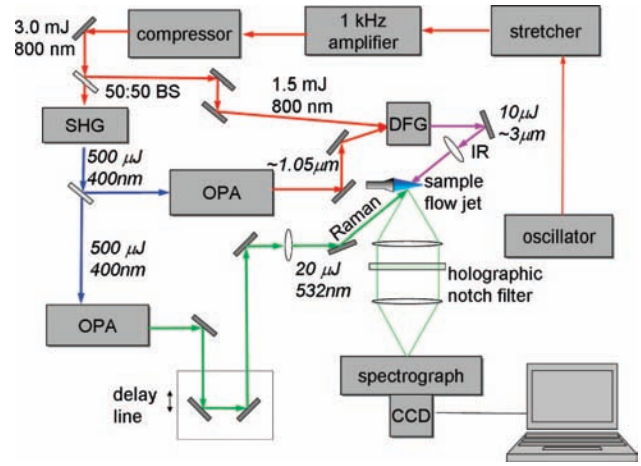

Figure 2. Schematic of laser apparatus for IR-Raman measurements. SHG: second-harmonic generating crystal; OPA: optical parametric amplifier; DFG: difference-frequency generation crystal; BS: beam splitter.

D. Anti-Stokes Raman Transients. Raman spectra were obtained in pairs, a signal at the indicated positive time delay and a background obtained at negative time delay (probe precedes IR pump). The Stokes spectrum was monitored to verify that the sample did not degrade during data acquisition. Anti-Stokes signals were converted into occupation number as follows. When the occupation number of a vibration of frequency ω is n_ω and the laser frequency is ω_L, the Stokes intensity is

$$I_{ST} \propto \omega_L(\omega_L - \omega)^3(n_\omega + 1)\sigma_R \quad (2)$$

and the anti-Stokes intensity is

$$I_{AS} \propto \omega_L(\omega_L + \omega)^3 n_\omega \sigma_R \quad (3)$$

where the proportionality constant is the same in both cases, and σ_R is the Raman cross-section at ω_L. When $n_\omega \ll 1$, the fraction of molecules in the excited-state is given by the fraction $= I_{AS}/I_{ST}$. This ratio was determined by correcting the detection system spectral response with a calibrated blackbody source.

E. Molecular Thermometer. The Stokes spectrum of D_2O was used as a molecular thermometer. As water temperature is increased from T_i to T_f, the Raman difference spectrum in the OH-stretch or OD-stretch region demonstrate a characteristic sigmoidal shape, including a dip near 2330 cm^{-1} whose amplitude increases with increasing temperature (cf. Figure 3 of ref 4). It is well-known this response originates from the blueshift because of weakened hydrogen bonding at higher temperature. The molecular thermometer effect was discussed in detail in prior studies of water[4,68] and of GLY in water.[33] The molecular thermometer employs temperature shifting of ground vibrational state transitions. At shorter times there are also vibrationally excited states created by the IR pump pulses, so that ground-state depletion and excited-state absorption effects are also present in the Stokes spectra.[3] Previously[33] we showed how a singular-value decomposition (SVD) analysis could be used to separate the Stokes spectra into an excited-state part which we do not use and a ground-state (molecular thermometer) part. We did not need to use this SVD method here. There is little overlap between the parent CH-stretch pumped by the IR pulses and the D_2O stretching spectrum, so the effects of excited states on the molecular thermometer spectrum was negligible.

We have also introduced an improvement to resolve a problem with our earlier study of GLY in water.[33] Because of

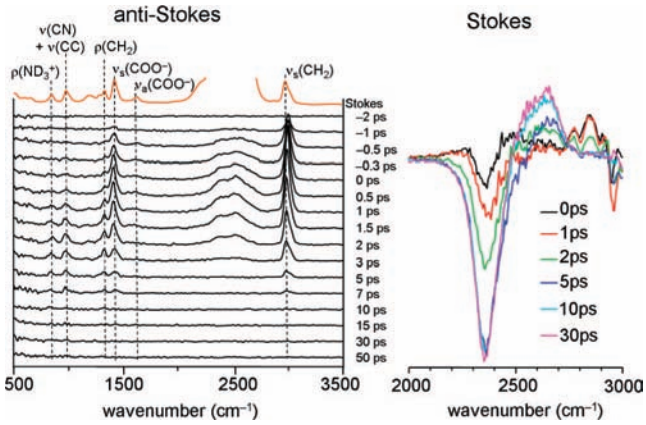

Figure 3. Transient Raman data for glycine-d_3 zwitterion in D_2O (GLY) with $\nu_s(CH_2)$ excitation. The parent and five daughter vibrations are seen in the anti-Stokes region (left). The response of the D_2O molecular thermometer is shown at right.

TABLE 1: Molecular Thermometer Parameters

	D_2O	glycine	NMAD	sodium BZ
pump wavenumber (cm^{-1})	2950	2970	2950	3050
fraction of D_2O excited	0.007	0.002	0.0036	0.0016
fraction of solute excited	–	0.021	0.034	0.032
molecular thermometer rise (ps)	1.8	7.2	4.9	8.0
observed vibrational energy loss (ps)	0.8	2.6	5.1	3.6

the spectral overlap between the solute CH-stretch and the very broad OH-stretch absorption of water, the IR pump pulse excited not only the solute but also the aqueous solvent. In that case part of the thermometer response resulted from VC of the solute, but an additional faster part was created by direct solvent IR pumping, so that the overall thermometer response appeared faster than solute VC. In the present work we have eliminated much of the solvent pumping effect by using D_2O, since there is less spectral overlap between the solute CH-stretch transitions and the solvent OD-stretch transition. The fraction of solute excited, which is listed in Table 1, is now always at least 1 order of magnitude greater than solvent excited. In addition we have developed a method for subtracting the remaining effects of direct solvent pumping. This was done by first performing a calibration experiment where the time-dependent thermometer response $T_{solvent}(t)$ of D_2O solvent was measured. In the calibration experiment the fraction of D_2O molecules pumped by the laser was n_{D2O} and the thermometer response $T_{solvent}(t)$ resulted from direct OD-stretch pumping only. Then, using GLY, NMA, or BZ solutions, we determined the fraction of D_2O molecules in solution n'_{D2O}, and the fraction of solute molecules n_{solute}, pumped by the IR pulse. We determined the observed thermometer response $T_{obs}(t)$ and then computed the thermometer response $T_{solute}(t)$ due to solute alone,

$$T_{solute}(t) = T_{obs}(t) - \frac{n'_{D2O}}{n_{D2O}} T_{solvent}(t) \quad (4)$$

4. Results

A. Glycine. Figures 3 and 4 show the GLY data. In the anti-Stokes spectra in Figure 3 we see the parent $\nu_s(CH_2)$ and five of the daughter vibrations (in order of descending wavenumber), $\nu_a(COO^-)$, $\nu_s(COO^-)$, $\rho(CH_2)$, $\nu(CN) + \nu(CC)$, and $\rho(ND_3^+)$. The vibrational wavenumbers and assignments[69] are summarized in Table 2. Figure 3 also shows Stokes data in the ν_{OD} region of the D_2O solvent. By combining Stokes and anti-Stokes

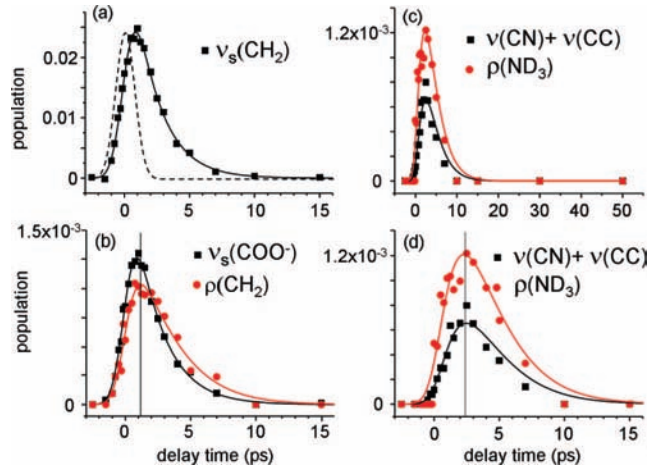

Figure 4. Anti-Stokes transients for glycine-d_3 in D_2O with $\nu_s(CH_2)$ excitation. The smooth curves are the fit to the three-stage model. The dashed curve in a is the apparatus time response. The vertical lines in b and d are visual guides. Part d shows the data in c on an expanded scale.

spectra, we find (Table 1) that the pump pulse excited 2.1% of the GLY solute and 0.2% of the D_2O solvent. Figure 4 shows the GLY anti-Stokes transients. The smooth curves are fits using the three-stage model with parameters listed in Table 2. Figure 4a shows the parent $\nu_s(CH_2)$ transient, which gives $\tau_{IVR} = 1.8(\pm0.2)$ ps. Figure 4b shows the midrange vibrations $\rho(CH_2)$ and $\nu_s(COO^-)$ which have $\tau_{ML} = 1.9(\pm0.2)$ ps. We also saw $\nu_{as}(COO^-)$, but because of its small σ_R it was difficult to get an accurate anti-Stokes transient. However, as far as we can tell, the lifetime and excitation fraction are close to what we see for $\nu_s(COO^-)$. Figures 4c and 4d show the two observed lower-energy vibration transients, which rise slower than either the parent or midrange vibrations and whose decays give $\tau_{LG} = 1.8(\pm0.2)$ ps. The quantum efficiencies extracted from these transients are listed in Table 2. The errors on the quantum efficiencies based on goodness of fit are ±20% except for the $L \rightarrow G$ efficiencies which, because of accumulations of errors, are estimated at ±30%.

B. NMA. The NMA-d data are shown in Figures 5−7. In the anti-Stokes data in Figure 5, we see the parent $\nu_s(CH_3)$ along with eight daughter vibrations, in order of descending wavenumber, amide I′, amide II′, CCH_3 ab, NCH_3 ab, $\nu_s(NC)$, amide III′, skeletal deformation, and amide IV′. Prime designates amide deuteration, and the vibrational assignments[31,70,71] are given in Table 2. Also in Figure 5 are the D_2O molecular thermometer data. The anti-Stokes transients are shown in Figure 6. The parent decay in Figure 6a gives $\tau_{IVR} = 1.2(\pm0.2)$ ps. The observed midrange daughter transients are shown in Figure 6b. Those decays gave $\tau_{ML} = 1.7(\pm0.2)$ ps. The amide II′ vibration demonstrates a faster rise than the other M vibrations indicating a degree of coherent coupling with the parent. The lower-energy transients are shown in Figures 6c and 6d. Those decays gave $\tau_{LG} = 2.8(\pm0.3)$ ps. The quantum efficiencies used to fit the data are listed in Table 2.

Figure 7 is a plot of the NMA anti-Stokes transients normalized to the same peak height to facilitate analysis of the rising edges. Keep in mind that any M or L vibration that is excited solely by parent IVR will have a rising edge that tracks the 1.2 ps parent lifetime. The amide II′ vibration rises much more quickly than this, which indicates that a substantial fraction of the amide II′ excitation is generated during the IR pump pulse. Since these excitations are created on time scales comparable to parent $\nu_s(CH_3)$ dephasing, the main excitation mechanism is

TABLE 2: Vibrational Assignments, Lifetimes, and Normalized Transfer Quantum Efficiencies[a]

	glycine-d_3 in D_2O					NMA-d in D_2O					benzoate anion in D_2O				
				quantum efficiency, %					quantum efficiency, %					quantum efficiency, %	
	lifetime T_1 (ps)	assignment[69]	freq (cm^{-1})	parent	mid-range	lifetime T_1 (ps)	assignment[70]	freq (cm^{-1})	parent	mid-range	lifetime T_1 (ps)	assignment[72]	freq (cm^{-1})	parent	mid-range
parent	1.8(±0.2)	$\nu_s(CH_2)$	2965			1.2(±0.2)	$\nu_s(CH_3)$	2945			1.0(±0.2)	ν_s(CH)	3050		
mid-range	1.9(±0.2)	$\nu_{as}(COO^-)$	1620	17		1.7(±0.2)	amide I′	1620	5		2.5(±0.2)	ν_s(CC)	1589	43	
		$\nu_s(COO^-)$	1412	18			amide II′	1490	17			$\nu_s(COO^-)$	1383	20	
		$\rho(CH_2)$	1323	33			CCH_3ab	1435	18						
lower	1.8(±0.2)	ν(CN)+ ν(CC)	966	17	50	2.8(±0.2)	NCH_3 sb	1192	11	0	2.7(±0.2)	ρ(CH)	1136	8	21
							ν_s(NC)	1117	6	25		ν_s(phenyl)	1001	10	30
		$\rho(ND_3^+)$	837	15	50		amide III′	975	3	40		δ_{oop}(CH)	836	6	12
							skel d	868	20	35		ρ(CCC)	625	13	37
							amide IV′	627	20	0					

[a] $\nu_s\nu_{as}$: symmetric, antisymmetric stretching; ρ: rocking; δ: bending, ab: in-plane antisymmetric bend; sb: symmetric bend; oop: out-of-plane; skel d: skeletal deformation.

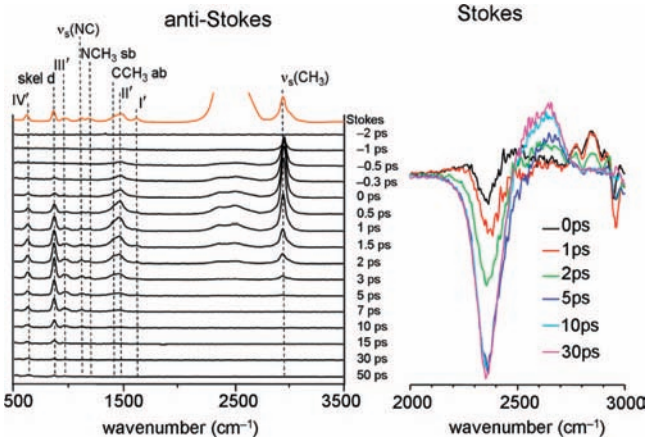

Figure 5. Transient Raman data for *N*-methylacetamide-*d* (NMA) in D_2O with $\nu_s(CH_3)$ excitation. The parent and eight daughter vibrations are seen in the anti-Stokes region (left). The response of the D_2O molecular thermometer is shown at right.

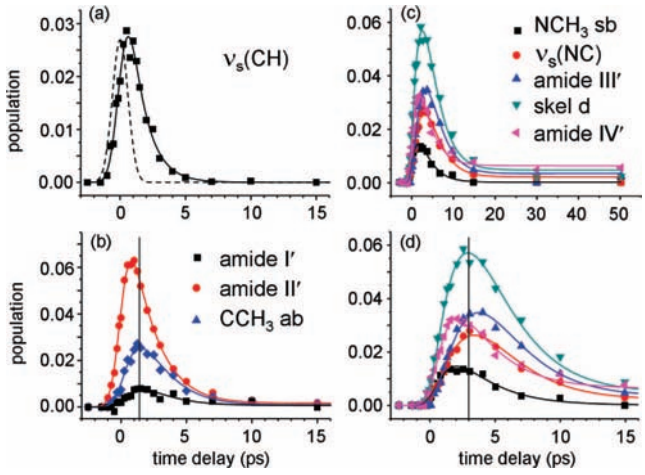

Figure 6. Anti-Stokes transients for *N*-methylacetamide-*d* (NMA) in D_2O with $\nu_s(CH_2)$ excitation. The smooth curves are the fit to the three-stage model. The dashed curve in a is the apparatus time response. The vertical lines in b and d are visual guides. Part d shows the data in c on an expanded scale.

the coherent coupling process described in Section 2. In our model, this excitation mechanism is described by a nonzero value of the α′ parameter.

C. Benzoate Anion. The BZ data are shown in Figures 8 and 9. In the anti-Stokes data we observe the parent ν_s(CH) along with six daughter vibrations, in descending order ν_s(CC),

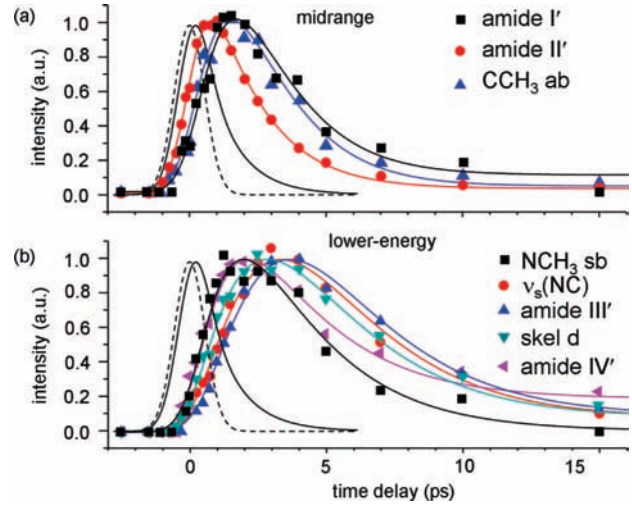

Figure 7. Anti-Stokes transients for NMA-*d* in D_2O with $\nu_s(CH_3)$ excitation, where each transient normalized to the same height to facilitate comparisons. The smooth dashed and solid curves represent the apparatus time response measured by nonlinear light scattering and the parent decay with $T_1 = 1.2$ ps, respectively.

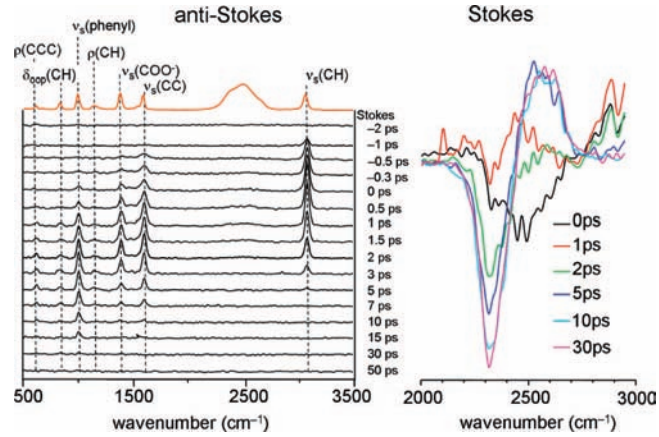

Figure 8. Transient Raman data for benzoate anion (BZ) in D_2O with ν_s(CH) excitation. The parent and five daughter vibrations are seen in the anti-Stokes region (left). The response of the D_2O molecular thermometer is shown at right.

$\nu_s(COO^-)$, ρ(CH), ν_s(phenyl), δ_{oop}(CH), and ρ(CCC). The anti-Stokes transients, vibrational assignments,[72] and fits using parameters in Table 2 are shown in Figure 9. The parent decay in Figure 9a gives $\tau_{IVR} = 1.0(\pm0.2)$ ps. The midrange vibrations in Figure 9b give $\tau_{ML} = 2.5(\pm0.2)$ ps, and the lower-energy

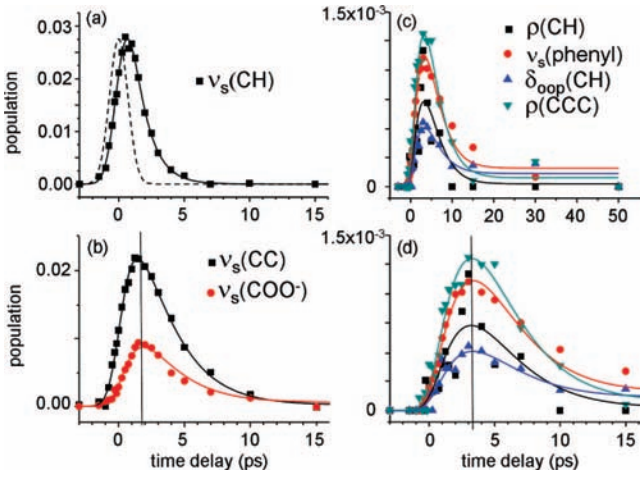

Figure 9. Anti-Stokes transients for benzoate anion (BZ) in D_2O with ν_s(CH) excitation. The smooth curves are the fit to the three-stage model. The dashed curve in a is the apparatus time response. The vertical lines in b and d are visual guides. Part d shows the data in c on an expanded scale.

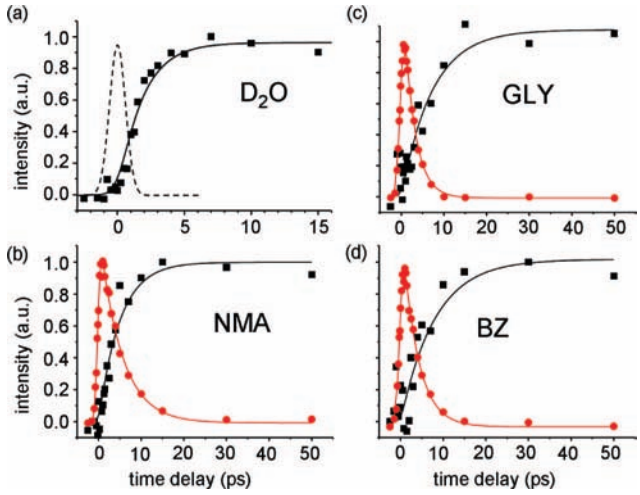

Figure 10. Molecular thermometer response. The molecular thermometer uses Stokes spectroscopy of the OD-stretch region of D_2O. Hydrogen bond weakening causes the transition to blueshift. (a) Response of pure D_2O pumped at 2950 cm^{-1} can be fit to an exponential with a 1.8 ps time constant. The dashed curve is the laser apparatus time response. (b−d) Thermometer data for NMA, GLY, and BZ after CH-stretch pumping (squares). The circles represent the total amount of vibrational energy observed via anti-Stokes probing of the solutes' vibrational transitions. In NMA the observed energy is representative of the solute cooling process detected by the thermometer response. In GLY and BZ the observed energy decays faster than the thermometer heats up, indicating energy is stored in a reservoir of unobserved vibrations. The observed energy is not representative of the solute cooling process for GLY and BZ.

vibrations in Figures 9c and 9d give $\tau_{LG} = 2.7(\pm 0.3)$ ps. In Figure 9b, the ν_s(CC) vibration rises faster than the other midrange vibration, indicating excitation via coherent coupling to the parent. The quantum efficiencies used to fit the data are listed in Table 2.

D. Molecular Thermometer. Figure 10 shows the molecular thermometer data. If the thermometer response results from the exponential decay of a single level, then the thermometer rise will be a rising exponential. If the response results from the accumulation of many individual level decay processes, each an exponential in time, then the thermometer rise should approach an error function.[46] We fit the thermometer rise with single-exponential functions, since the quality of the data does not justify a more sophisticated treatment. Figure 10a is the result for pure D_2O. As shown in Table 1, the intrinsic response of the D_2O molecular thermometer, measured by pumping ν(OD) of pure D_2O at 2950 cm^{-1} with an excited-state concentration of 0.7%, is characterized by 1.8 ps time constant. This is just about what would be expected based on a ν_{OD} lifetime[68] of 1.4 ps and a thermalization time constant[4,73−76] of ∼0.5 ps. When solutes were added, the fraction of ν(OD) excited by the IR pulse (shown in Table 1) decreased because of the competition with solute absorption. The ν(OD) excitation fraction and the 1.8 ps time dependence for pure D_2O were used to subtract the part of the thermometer response due to direct ν(OD) pumping. The resulting molecular thermometer responses due to solute pumping alone are shown in Figures 10b−d. The time constants for the molecular thermometer rises are given in Table 1. The fastest vibrational cooling denoted by the thermometer rise, 4.9 ps, was observed with NMA. With GLY and BZ, the time constants for VC were 7.2 and 8.0 ps, respectively.

E. Observed Vibrational Energy. Using the anti-Stokes data in Figures 4, 6, and 8, we determined the time-dependence of the observed vibrational energy using the formula,

$$E_{vib}^{obs}(t) = \sum_{i=1}^{\#obs} h\nu_i n_i(t) \quad (5)$$

The results were decaying curves for each solute that could be reasonably fit to an exponential decay, as shown in Figures 10b−d. The time constants for energy loss in the observed vibrations are listed in Table 1.

4. Discussion

In this section we discuss the nature of the initial state "CH-stretch" prepared by the IR pulse in GLY, NMA, and BZ, the details of vibrational energy flow revealed by anti-Stokes Raman spectroscopy, and the energy dissipation process from the point of view of the solute and solvent.

A. The Initial State. The IR pump pulse is tuned to a CH-stretch transition. Since CH or CD stretching transitions have been considered as probes of protein dynamics, the question arises whether the excitation should be thought of as localized on CH_3 (NMA), CH_2 (GLY), or CH (BZ), or whether it should be viewed as delocalized over a larger part of the molecule.

In NMA, $CH_3-CO-ND-CH_3$, the parent 2945 cm^{-1} $\nu_s(CH_3)$ is an admixture of both methyl groups. The anti-Stokes data provides evidence for coherent coupling with the 1490 cm^{-1} amide II′ vibration. Amide II vibrations are usually viewed as a mixture of NH-bend and CN-stretch character. Thus, this parent excitation should be viewed as delocalized throughout the entire molecule. In GLY, $ND_3^+-CH_2-CO_2^-$, there is no evidence for *M* or *L* vibrations that have much coherent coupling with the parent 2965 cm^{-1} $\nu_s(CH_2)$, so our measurements do not support the idea that the parent methylene excitation extends to the amine or carboxylate groups. In BZ, $C_6H_5-CO_2^-$, the parent was the 3050 cm^{-1} ν_s(CH) stretch, which is delocalized among all five CH subunits of the aromatic ring. The parent is coherently coupled with the 1589 cm^{-1} symmetric ring C−C stretching mode, so the parent involves an admixture of phenyl CH-stretch and CC-stretch character. Thus, in NMA and BZ, the parent CH-stretch excitation should be viewed as reporting perturbations to most, if not all, of the solute molecule.

B. Vibrational Energy Flow. ***1. Glycine-d_3 Zwitterion.*** Table 2 shows that in the initial 1.8 ps parent IVR process, the transfer quantum efficiency is about the same for the five

TABLE 3: Assignments,[a] Frequencies and Vibrational Relaxation Time Constants of Observed Raman Transitions of Glycine Zwitterion in Water and D_2O

h_3-glycine zwitterion	wavenumber (cm^{-1})	glycine-d_3 zwitterion	wavenumber (cm^{-1})	h_3-glycine time constants	glycine-d_3 time constants
$\nu_s(CH_2)$	2980	$\nu_s(CH_2)$	2965	τ_{IVR}=0.8(±0.2)ps	τ_{IVR}=1.8(±0.2)ps
$\nu_{as}(COO^-)$	1586	$\nu_a(COO^-)$	1620		
$\nu_s(COO^-)$	1410	$\nu_s(COO^-)$	1412	τ_{ML} =1.0(±0.2)ps	τ_{ML} =1.9(±0.2)ps
$\rho(CH_2)$	1313	$\rho(CH_2)$	1323		
$\rho(NH_3^+)$	1107	ν(CN +ν(CC)	966		
ν(CN)	1010	$\rho(ND_3^+)$	837	τ_{LG} =1.2(±0.3)ps	τ_{LG} =1.8(±0.3)ps
ν(CC)	887				

[a] Taken from ref 69.

observed daughters except for the coherently coupled $\rho(CH_2)$ which receives about twice as much energy. In the 1.9 ps *M* to *L* step, the *M* energy is split about equally between the two observed *L* vibrations. The *L* vibration relaxation occurs in 1.8 ps. Each of the three stages of VC occurs with a 1.8−1.9 ps time constant. GLY is thus an example of a solute where the parent energy is distributed among first- and second-tier daughter vibrations in an approximately statistical manner. There is no evidence for a single strongly dominant relaxation pathway.

As a result of our previous work[33] on glycine in H_2O, we can make a comparison between glycine in normal and heavy water. This comparison illustrates the usefulness of the three stage model. Instead of trying to compare detailed vibrational parameters of similar or corresponding energy levels, we can compare the time constants and relaxation mechanisms of the three stages. As shown in Table 3, in water the three time constants for GLY are noticeably faster. It is important to resist the temptation to describe this as a solvent effect, because GLY in H_2O is not just a different solvent, it is a different molecule, $NH_3^+CH_2-CO_2^-$ as opposed to $ND_3^+CH_2-CO_2^-$, and the energy levels of h_3-glycine are upshifted from glycine-d_3 by isotope mass effects. As shown in Table 3, the most significant effect on the observed vibrations is the NH_3^+/ND_3^+ rocking mode, 1107 cm^{-1} in water and 837 cm^{-1} in D_2O. This rocking vibration can be viewed as an *M* vibration in h_3-glycine but an *L* vibration in glycine-d_3. We attribute the faster IVR in h_3-glycine to its higher-energy daughter vibrations, which facilitate parent IVR. The faster *M* to *L* relaxation of h_3-glycine is attributed to having more *M* vibrations available to dissipate energy. The *L* to *G* relaxation, by contrast, is attributed to solvent effects, since *L* vibrations relax directly to excitations of the aqueous bath. This faster *L* to *G* relaxation in water might be a consequence of better coupling between *L* vibrations and water librons. In water the libron is centered near 700 cm^{-1} with a fwhm of ∼300 cm^{-1}, and in D_2O the libron is centered near 540 cm^{-1} with a fwhm of ∼200 cm^{-1}.[77,78]

2. N-Methylacetamide-d. In NMA, during parent IVR only a small fraction of the parent energy flows into amide I′, ν_s(NC), or amide III′ vibrations. During the *M* to *L* relaxation, practically none of the midrange energy flows into NH_3 sb or amide IV′ vibrations. So NMA differs quite a bit from GLY in the sense that the IVR and the *M* to *L* pathways are more specific.

The amide I′ vibration of NMA, which is one of our *M* states, has been studied by IR pump−probe and 2D IR methods by several researchers,[79−81] so to a degree a comparison can be made to our IR-Raman measurements. The caveat is that in these cited works, amide I′ was pumped by a short IR pulse, whereas in our experiments, amide I′ was pumped by IVR from the parent $\nu_s(CH_3)$. In magic-angle pump−probe measurements (magic-angle measurements eliminate the rotational relaxation contribution), biexponential decays were seen where the faster part was reported to be 200 or 450 fs and the slower part 900 fs or 4 ps. The faster part was interpreted as arising from vibrational energy exchange among nearby states and the slower part as loss of vibrational excitation {DeFlores, 2006 #2537; Hamm, 1998 #523}. In our experiments we do not see this faster part because the amide I′ is pumped not by 100−200 fs duration IR pulse but by the 1.2 ps decay of the parent *P*. The effects of this redistribution process would appear in our model in the ϕ_{PMi} quantum efficiencies. These efficiencies would reflect both the efficiency of $P \rightarrow M_i$ energy transfer and also any fast redistribution among M_i states. Our 1.7 ps time constant for VR of the observed *M* states is consistent with the interpretation of the slower part of the IR pump−probe data due to vibrational energy loss from the *M* tier.

3. Benzoate. The most dramatic result of the BZ study is the large difference in time scales for relaxation of phenyl vibrational excitations in an aqueous medium versus neat benzene.[64] The BZ lifetimes are all in the 1−3 ps time range, whereas in liquid benzene observed vibrational lifetimes are in the 8−100 ps time range.[64] Since vibrational lifetimes are determined by fluctuating forces acting on excited vibrations, the much shorter lifetimes in BZ should be attributed fluctuating forces due to fluctuating charges and fluctuating hydrogen bonding present in the water-anion system[82] but not in neat benzene.

In the BZ IVR process, after a phenyl CH-stretch transition is pumped, more of the parent energy is channeled to the *M* vibrations than to the *L* vibrations, with the strongly coupled ν_s(CC) vibration receiving nearly half of the observed excitations. In the *M* to *L* stage, energy is about evenly distributed among three of the lower-energy vibrations, but the fourth, δ_{oop}(CH), receives noticeably less energy. Thus, the energy relaxation pathways in BZ appear to be the most specific of the three solutes studied here. The specificity of the VR pathways is attributed to the more rigid and more symmetric phenyl ring structure, as opposed to the low-symmetry flexible amino acid or peptide backbone.

C. Vibrational Cooling. According to Table 1, the overall time constant for thermalization of the parent vibration energy is ∼5 ps for NMA and ∼8 ps for GLY and BZ. Thus, informed speculation would suggest that energy deposited in the backbone or in flexible side chains of polypeptides would be thermalized in ∼5 ps, and even energy deposited in rigid side chain structures would thermalize within <10 ps.

Table 1 also shows that dissipation of the observed energy in the strongly Raman-active vibrations of NMA is representative of the overall thermalization process monitored by the molecular thermometer, in the sense that the two probes demonstrates the same decay lifetime. However, the GLY and BZ observed vibrational energy loss is about three time faster than the thermalization. Thus, the strongly Raman-active NMA vibrations do an excellent job of representing energy flow through the solute, whereas the GLY and BZ vibrations do not.

The GLY and BZ molecular thermometer response is slower than the observed vibrational energy. This means there must be at least one unobserved state that is releasing energy to the surroundings more slowly than the Raman-active states we observe. The representative versus nonrepresentative nature of the observed NMA vibrations versus GLY and BZ might result from the nature of specific vibrational pathways, but there might be a simpler statistical explanation. NMA is the molecule where we observe the largest number of vibrations, nine, compared to five for GLY and six for BZ. The larger the number of observed vibrations, the more likely the observed vibrational energy will be representative of the entire molecule.

5. Summary and Conclusion

We used time-resolved Raman spectroscopy to monitor vibrational energy flow through GLY, NMA, and BZ solutes in an aqueous (D_2O) solvent by probing vibrational energy of the solute and by using the aqueous medium as a molecular thermometer. The details of energy flow within the solute vibrations was described using a three-stage model for VR. This three-stage model did an excellent job of describing vibrational energy in these three solutes and also in GLY in H_2O studied previously. The theoretical basis for the model suggests it will be useful to describe vibrational energy in the common building blocks of biological systems such as proteins (amino acids), nucleic acids (nucleotides, sugars), and carbohydrates (sugars). The utility of the model was demonstrated by showing how it facilitated comparison of the VR processes of the three solutes and a comparison of GLY in water and heavy water.

The dissipation of vibrational energy from the solutes occurred with time constants ranging from 5 to 8 ps. Even the rigid and highly symmetric phenyl group of BZ dissipated its energy within 8 ps, much faster than one would expect based on studies of liquid benzene. The VR process in GLY was seemingly statistical, in that every vibration received about the same fraction of the initial excitation. In NMA there were at least two vibrations which received less energy than the others, so the VR process was more specific than in GLY. In BZ the relaxation was even more specific, with one channel, phenyl CH-stretch to ring symmetric CC-stretch, dominating.

Although the parent excitations were created by pumping "CH-stretch" transitions, Raman probing showed that the excitations were in all three cases coherently coupled with states at about one-half the energy, so that the CH-stretch involved atomic motions over the entire molecule (NMA), over most of the molecule (the GLY methylene and carboxylate) or over the entire side chain (phenyl of BZ).

With Raman probing, we observe only vibrations with the largest σ_R. We have shown that in NMA, where we observe the greatest number of vibrations (9 of 30 total), energy flow through the observed vibrations is entirely representative of energy in the molecule, but in GLY and BZ the loss of energy in the observed vibrations was about three times slower than the molecular dissipation process observed by the molecular thermometer, so the observed GLY and BZ vibrations do not accurately represent vibrational energy flow through the molecule.

Acknowledgment. This material is based upon work supported by the National Science Foundation under award DMR 0504038, and the Air Force Office of Scientific Research under award FA9550-06-1-0235.

References and Notes

(1) Dlott, D. D. *Chem. Phys.* **2001**, *266*, 149.
(2) Laubereau, A.; Kaiser, W. *Rev. Mod. Phys.* **1978**, *50*, 607.
(3) Wang, Z.; Pang, Y.; Dlott, D. D. *Chem. Phys. Lett.* **2004**, *397*, 40.
(4) Wang, Z.; Pang, Y.; Dlott, D. D. *J. Phys. Chem. A* **2007**, *111*, 3196.
(5) Seilmeier, A.; Scherer, P. O. J.; Kaiser, W. *Chem. Phys. Lett.* **1984**, *105*, 140.
(6) Graham, P. B.; Matus, K. J. M.; Stratt, R. M. *J. Chem. Phys.* **2004**, *121*, 5348.
(7) Lian, T.; Locke, B.; Kholodenko, Y.; Hochstrasser, R. M. *J. Phys. Chem.* **1994**, *98*, 11648.
(8) Henry, E. R.; Eaton, W. A.; Hochstrasser, R. M. *Proc. Natl. Acad. Sci. U.S.A.* **1986**, *83*, 8982.
(9) Uchida, T.; Kitagawa, T. *Acc. Chem. Res.* **2005**, *2005*, 662.
(10) Lingle, R. J.; Xu, X.; Zhu, H.; Yu, S.-C.; Hopkins, J. B. *J. Phys. Chem.* **1991**, *95*, 9320.
(11) Lingle, R. J.; Xu, X. B.; Zhu, H. P.; Yu, S.-C.; Hopkins, J. B. *J. Am. Chem. Soc.* **1991**, *113*, 3992.
(12) Li, P.; Sage, J. T.; Champion, P. M. *J. Chem. Phys.* **1992**, *97*, 3214.
(13) Li, P.; Champion, P. M. *Biophys. J.* **1994**, *66*, 430.
(14) Ye, X.; Demidov, A.; Rosca, F.; Wang, W.; Kumar, A.; Ionascu, D.; Zhu, L.; Barrick, D.; Wharton, D.; Champion, P. M. *J. Phys. Chem. A* **2003**, *107*, 8156.
(15) Fujisaki, H.; Straub, J. E. *Proc. Natl. Acad. Sci. U.S.A.* **2005**, *102*, 6726.
(16) Miller, R. J. D. *Annu. Rev. Phys. Chem.* **1991**, *42*, 581.
(17) Simpson, M. C.; Peterson, E. S.; Shannon, C. F.; Eads, D. D.; Friedman, J. M.; Cheatum, C. M.; Ondrias, M. R. *J. Am. Chem. Soc.* **1997**, *119*, 5110.
(18) Challa, J. R.; Gunaratne, T. C.; Simpson, M. C. *J. Phys. Chem. B* **2006**, *110*, 19956.
(19) Sato, A.; Gao, Y.; Kitagawa, T. *Proc. Natl. Acad. Sci U.S.A.* **2007**, *104*, 9627.
(20) Gao, Y.; Koyama, M.; El-Mashtoly, S. F.; Hayashi, T.; Harada, K.; Mizutani, Y.; Kitagawa, T. *Chem. Phys. Lett.* **2006**, *429*, 239.
(21) Gao, Y.; El-Mashtoly, S. F.; Pal, B.; Hayashi, T.; Harada, K.; Kitagawa, T. *J. Biol. Chem.* **2006**, *281*, 24737.
(22) Bu, L.; Straub, J. E. *J. Phys. Chem. B* **2003**, *107*, 10634.
(23) Zhang, Y.; Fujisaki, H.; Straub, J. E. *J. Phys. Chem. B* **2007**, *111*, 3243.
(24) Sagnella, D. E.; Straub, J. E. *J. Phys. Chem. B* **2001**, *105*, 7057.
(25) Hill, J. R.; Tokmakoff, A.; Peterson, K. A.; Sauter, B.; Zimdars, D.; Dlott, D. D.; Fayer, M. D. *J. Phys. Chem.* **1994**, *98*, 11213.
(26) Peterson, K. A.; Hill, J. R.; Tokmakoff, A.; Sauter, B.; Zimdars, D.; Dlott, D. D.; Fayer, M. D. Vibrational dynamics at the active site of myoglobin: Picosecond infrared free-electron-laser experiments. In *Ultrafast Phenomena IX*; Barbara, P. F., Ed.; Springer-Verlag: Berlin, 1994; Vol. 60; p 445.
(27) Peterson, K. A.; Boxer, S. G.; Decatur, S. M.; Dlott, D. D.; Fayer, M. D.; Hill, J. R.; Rella, C. W.; Rosenblatt, M. M.; Suslick, K. S.; Ziegler, C. J. Vibrational relaxation of carbon monoxide in myoglobin mutants and model heme compounds. I. *Time-Resolved Vib. Spectrosc. VII* **1996**, 173.
(28) Owrutsky, J. C.; Li, M.; Locke, B.; Hochstrasser, R. M. *J. Phys. Chem.* **1995**, *99*, 4842.
(29) Fujisaki, H.; Straub, J. E. *J. Phys. Chem. B* **2007**, *111*, 12017.
(30) Hamm, P.; Lim, M.; Hochstrasser, R. M. *Biophys. J.* **1998**, *74*, A332.
(31) DeFlores, L. P.; Ganim, Z.; Ackley, S. F.; Chung, H. S.; Tokmakoff, A. *J. Phys. Chem. B* **2006**, *110*, 18973.
(32) Peterson, K. A.; Rella, C. W.; Engholm, J. R.; Schwettman, H. A. *J. Phys. Chem. B* **1999**, *103*, 557.
(33) Shigeto, S.; Dlott, D. D. *Chem. Phys. Lett.* **2007**, *447*, 134.
(34) Gruebele, M. *Theor. Chem. Acc.* **2003**, *109*, 56.
(35) Gruebele, M. *Adv. Chem. Phys.* **2000**, *114*, 193.
(36) Bigwood, R.; Gruebele, M. *Chem. Phys. Lett.* **1995**, *235*, 604.
(37) Leitner, D. M.; Gruebele, M. *Mol. Phys.* **2008**, *106*, 433.
(38) Cremeens, M. E.; Fujisaki, H.; Zhang, Y.; Zimmermann, J.; Sagle, L. B.; Matsuda, S.; Dawson, P. E.; Straub, J. E.; Romesberg, F. E. *J. Am. Chem. Soc.* **2006**, *128*, 6028.
(39) Naraharisetty, S. R. G.; Kurochkin, D. V.; Rubtsov, I. V. *Chem. Phys. Lett.* **2007**, *437*, 262.
(40) Kumar, K.; Sinks, L. E.; Wang, J.; Kim, Y. S.; Hochstrasser, R. M. *Chem. Phys. Lett.* **2006**, *432*, 122.
(41) Kinnaman, C. S.; Cremeens, M. E.; Romesberg, F. E.; Corcelli, S. A. *J. Am. Chem. Soc.* **2006**, *128*, 13334.
(42) Mirkin, N. G.; Krimm, S. *J. Phys. Chem. A* **2007**, *111*, 5300.
(43) Deàk, J. C.; Rhea, S. T.; Iwaki, L. K.; Dlott, D. D. *J. Phys. Chem. A* **2000**, *104*, 4866.
(44) Graener, H.; Zürl, R.; Hofmann, M. *J. Phys. Chem.* **1997**, *101*, 1745.
(45) Shigeto, S.; Pang, Y.; Fang, Y.; Dlott, D. D. *J. Phys. Chem. B* **2008**, *112*, 232.
(46) Hill, J. R.; Dlott, D. D. *J. Chem. Phys.* **1988**, *89*, 830.
(47) Hill, J. R.; Dlott, D. D. *J. Chem. Phys.* **1988**, *89*, 842.

(48) Iwaki, L.; Dlott, D. D. Vibrational energy transfer in condensed phases. In *Encyclopedia of Chemical Physics and Physical Chemistry*; Moore, J. H., Spencer, N. D., Eds.; IOP Publishing Ltd.: London, 2001; p 2717.

(49) Hoffman, G. J.; Imre, D. G.; Zadoyan, R.; Schwentner, N.; Apkarian, V. A. *J. Chem. Phys.* **1993**, *98*, 9233.

(50) McDonald, J. D. *Annu. Rev. Phys. Chem.* **1979**, *30*, 29.

(51) Nitzan, A.; Jortner, J. *Mol. Phys.* **1973**, *25*, 713.

(52) Chen, S.; Lee, I.-Y. S.; Tolbert, W.; Wen, X.; Dlott, D. D. *J. Phys. Chem.* **1992**, *96*, 7178.

(53) Wang, Z.; Pang, Y.; Dlott, D. D. *J. Phys. Chem. B* **2006**, *110*, 201150.

(54) Deàk, J. C.; Iwaki, L. K.; Dlott, D. D. *Chem. Phys. Lett.* **1998**, *293*, 405.

(55) Deàk, J. C.; Iwaki, L. K.; Dlott, D. D. *J. Phys. Chem.* **1998**, *102*, 8193.

(56) Deàk, J. C.; Iwaki, L. K.; Dlott, D. D. *J. Phys. Chem. A* **1999**, *103*, 971.

(57) Deàk, J. C.; Iwaki, L. K.; Rhea, S. T.; Dlott, D. D. *J. Raman Spectrosc.* **2000**, *31*, 263.

(58) Felker, P. M.; Zewail, A. H. *Phys. Rev. Lett.* **1984**, *53*, 501.

(59) Tokmakoff, A.; Kowk, A. S.; Urdahl, R. S.; Francis, R. S.; Fayer, M. D. *Chem. Phys. Lett.* **1995**, *234*, 289.

(60) Iwaki, L. K.; Dlott, D. D. *J. Phys. Chem. A* **2000**, *104*, 9101.

(61) Velsko, S.; Oxtoby, D. W. *J. Chem. Phys.* **1980**, *72*, 2260.

(62) Oxtoby, D. W. Vibrational population relaxation in liquids. In *Photoselective Chemistry Part 2*; Jortner, J., Levine, R. D., Rice, S. A., Eds.; Wiley: New York, 1981; Vol. 47; p 487.

(63) Chen, S.; Hong, X.; Hill, J. R.; Dlott, D. D. *J. Phys. Chem.* **1995**, *99*, 4525.

(64) Iwaki, L. K.; Deàk, J. C.; Rhea, S. T.; Dlott, D. D. *Chem. Phys. Lett.* **1999**, *303*, 176.

(65) Iwaki, L. K.; Dlott, D. D. *Chem. Phys. Lett.* **2000**, *321*, 419.

(66) Wang, Z.; Pakoulev, A.; Pang, Y.; Dlott, D. D. *J. Phys. Chem. A* **2004**, *108*, 9054.

(67) Wang, Z.; Pakoulev, A.; Pang, Y.; Dlott, D. D. *Chem. Phys. Lett.* **2003**, *378*, 281.

(68) Steinel, T.; Asbury, J. B.; Zheng, J. R.; Fayer, M. D. *J. Phys. Chem. A* **2004**, *108*, 10957.

(69) Derbel, N.; Hernández, B.; Pflüger, F.; Liquier, J.; Geinguenaud, F.; Jadane, N.; Ben Lakhdar, Z.; Ghomi, M. *J. Phys. Chem. B* **2007**, *111*, 1470.

(70) Chen, X. G.; Schweitzer-Stenner, R.; Asher, S. A.; Mirkin, N. G.; Krimm, S. *J. Phys. Chem.* **1995**, *99*, 3074.

(71) Kubelka, J.; Keiderling, T. A. *J. Phys. Chem. A* **2001**, *105*, 10922.

(72) Green, J. H. S.; Kynaston, W.; Lindsey, A. S. *Spectrochim. Acta* **1961**, *16*, 486.

(73) Kropman, M. F.; Nienhuys, H.-K.; Woutersen, S.; Bakker, H. J. *J. Phys. Chem. A* **2001**, *105*, 4622.

(74) Lock, A. J.; Woutersen, S.; Bakker, H. J. *J. Phys. Chem. A* **2001**, *105*, 1238.

(75) Ashihara, S.; Huse, N.; Espagne, A.; Nibbering, E. T. J.; Elsaesser, T. *Chem. Phys. Lett.* **2006**, *424*, 66.

(76) Elsaesser, T.; Ashihara, S.; Huse, N.; Espagne, A.; Nibbering, E. *J. Phys. Chem. A* **2007**, *111*, 743.

(77) Walrafen, G. E.; Blatz, L. A. *J. Chem. Phys.* **1973**, *59*, 2646.

(78) Walrafen, G. E.; Hokmabadi, M. S.; Yang, W. H. *J. Phys. Chem.* **1988**, *92*, 2433.

(79) DeCamp, M. F.; DeFlores, L.; McCracken, J. M.; Tokmakoff, A.; Kwac, K.; Cho, M. *J. Phys. Chem.* **2005**, *109*, 11016.

(80) Hamm, P.; Lim, M.; Hochstrasser, R. M. *J. Phys. Chem. B* **1998**, *102*, 6123.

(81) Zanni, M. T.; Asplund, M. C.; Hochstrasser, R. M. *J. Chem. Phys.* **2001**, *114*, 4579.

(82) Owrutsky, J. C.; Raftery, D.; Hochstrasser, R. M. *Annu. Rev. Phys. Chem.* **1994**, *45*, 519.

JP8062228